Active Self-Tuning Metasurface With Enhanced Absorbing Frequency Range for Suppression of High-Power Surface Currents

Sanghoon Kim, *Member, IEEE*, Aobo Li, *Member, IEEE*, Jiyeon Lee, *Member, IEEE*, and Daniel F. Sievenpiper, *Fellow, IEEE*

***Abstract*— We demonstrate a unique metamaterial surface that actively tunes its resonance frequency to match the frequency of incident electromagnetic waves, providing a broadband self-tuning absorber. The metasurface is constructed with nonlinear circuit components and is capable of detecting the incoming signals and adapting its resonant frequency without any external control. The fabricated prototype achieves 70% of −3 dB fractional frequency range compared with the intrinsic limit of around 5% for a passive absorbing surface of the same thickness. Its performance is experimentally verified by measuring absorption as a function of frequency with the self-tuning circuits turned on or off to demonstrate the self-tuning capability and the increase in the absorption frequency range. The measurements were performed for both TM and TE polarizations and various oblique incident angles. The proposed metasurface has a threshold power level for the absorption of incident waves and only absorbs high-power interfering signals while allowing small signals, such as for communications.**

***Index Terms*— Electromagnetic devices, electromagnetic metamaterials, electromagnetic wave absorption, nonlinear circuits.**

I. Introduction

CONVENTIONAL absorbing mediums can be categorized as broadband absorbers [1] that are formed by electrically thick absorbing materials, such as pyramidal absorbing foams or magnetic radar absorbing materials [2], or resonant absorbers that are constructed by combining resistive materials with a quarter-wavelength delay structure or other patterned resonant materials, such as the frequency-selective surface [3], Salisbury screen [4]–[6], or circuit analog absorbers [7]. For many applications, broadband absorbers are prohibitively thick, costly, and heavy, while resonant absorbers are not practical due to their limited bandwidth. Thus, there is a demand for a novel broadband absorber that can exceed the limitations of these tradeoffs, providing a broad absorbing bandwidth in an electrically thin structure.

As electrically thin absorbers, metamaterials have rapidly developed in recent years in many scientific and engineering fields [8], [9] due to their unique electromagnetic properties. A specific type of metamaterial composed of planar metallic unit cells arranged in a subwavelength periodic lattice is often called a metasurface [10]–[12]. The electromagnetic properties of the metasurface are defined by its surface impedance, which relates to the tangential components of electric and magnetic fields on the surface. The effective surface impedance is determined by using electromagnetic modeling tools to calculate the reflection phase from a single unit cell of the 2-D array of conductive patches on a grounded dielectric substrate. It can be understood by considering the unit cells as an array of effective LC resonant circuits [13], [14]. Near the resonance frequency, the surface impedance is significantly higher than the impedance of free space, and adding lossy materials or loaded lossy components can make it an effective microwave absorber near its resonance frequency [15]–[22]. With deploying active RF components, such as transistors [23] and varactors [24]–[29], the surface impedance of the metasurface can be adjusted by applying the external control manners to tune its resonance frequency. However, the bandwidth of such a structure is fundamentally limited by its thickness, and it gives difficulties in practical applications. Moreover, most of the microwave absorbers have focused either to suppress transmission or reduce and scatter reflection for radar absorbing applications [30]–[32], but the absorbers have to play another crucial role to protect sensitive electronics, such as antenna and radar systems from triggering malfunctions or even permanent damages when the incident power level is high enough, and interfered with leakage currents through apertures or openings on the conductive enclosures that support the system [23], [33], [34]. In this article, we introduce the novel absorbing metasurface that enables to enhance the absorbing frequency range and effectively suppress the surface currents. The metasurface can adaptively tune its resonance frequency to match that of the incoming waves without any external control system, thus forming a *self-tuning* metasurface. This article is organized as follows. Section I introduces the application and limit of the modern microwave absorbers and the unique performance of the proposed metasurface absorber as applying the self-tuning concept. Section II presents the bandwidth limitation of the electrical thin substrate by the analytical approach. In addition, the principle and analysis of the self-tuning metasurface are addressed to overcome the frequency range limitation. Section III describes the numerical method by cosimulation and closed-loop measurement procedures for the fabricated prototype surface. Section IV shows the experiment results

Manuscript received March 29, 2020; revised August 18, 2020; accepted September 14, 2020. Date of publication October 27, 2020; date of current version May 5, 2021. This work was supported by the Office of Naval Research under Grant N00014-15-1-2062. *(Corresponding author: Sanghoon Kim.)*

The authors are with the Electrical and Computer Engineering Department, University of California San Diego, La Jolla, CA 92093-0021 USA (e-mail: phd.sanghoon.kim@gmail.com).

Color versions of one or more of the figures in this article are available online at https://ieeexplore.ieee.org.

Digital Object Identifier 10.1109/TAP.2020.3032834

of the self-tuning metasurface with the enhanced absorbing frequency range. Section V delivers a final conclusion.

II. Principle and Analysis of Self-Tuning Metasurface

A. Bandwidth of Electrical Thin Substrate

The proposed metasurface is constructed of an artificial impedance surface consisting of a conductive array of patches on a grounded dielectric substrate with shorted vias between the metallic patches and ground, thus forming a high-impedance surface (HIS) [35]. The HIS has its property to suppress surface waves and enables it to highly attenuate incoming fields near the band edge of the forbidden gap, while losses are loaded. The bandwidth of the HIS can be defined as considering the surface as 2-D resonators that store incoming electromagnetic energies [36]. The quality factor of a resonator, Q, including the loss term, is given by

$$Q = 2\pi \frac{Energy\ stored}{Energy\ lost\ per\ cycle}. \tag{1}$$

The lossy HIS can be modeled to a parallel *RLC* circuit as an equivalent circuit model [35] with the resonance frequency $\omega_0 = 1/\sqrt{LC}$, in which L is the equivalent inductance determined by the thickness of the surface, C is the equivalent capacitance of the gap between neighboring patches, and R is the equivalent resistance from the dielectric loss of substrate and loaded resistance at the gaps. The equivalent L and C can be expressed to I of the current through the inductor and V of the voltage across the capacitor, respectively. In addition, by substituting the resonance frequency ω_0, the simplified quality factor can be expressed in terms of R, L, and C components, $Q = R\sqrt{C/L}$. The bandwidth of the impedance can be obtained as the inverse of the quality factor and by substituting the characteristic impedance η for R

$$BW = \frac{1}{Q} = \frac{1}{R}\sqrt{\frac{L}{C}} = \sqrt{\frac{\epsilon_0}{\mu_0}}\sqrt{\frac{L}{C}} \tag{2}$$

where ϵ_0 and μ_0 are the permittivity and permeability in free space. In (2), the inductance of the surface, L, can be determined by permeability μ and thickness t of substrate [37], so the bandwidth can be obtained for an electrically thin ($t \ll \lambda_0$), nonmagnetic ($\mu_r = 1$), and grounded resonator surface

$$BW = \frac{2\pi\mu_r t}{\lambda_0} = \frac{2\pi}{\lambda_0} t \tag{3}$$

where λ_0 is free space wavelength at the resonance frequency. In (3), it results in that the bandwidth is dominantly determined by the thickness of the substrate and independent of the permittivity of the dielectric slab. In other words, it is not possible to make a broadband absorber with an arbitrarily thin substrate. Due to this intrinsic limitation, the practical applications of metasurface absorbers are limited. For instance, the thickness of the proposed metasurface is 1.575 mm, and it has about 7% fractional bandwidth at 2.2 GHz from (3), which is the lower band edge.

To exceed the fundamental bandwidth limit for a passive surface, several intriguing approaches are provided by defining resistive loaded [17], multilayer loaded [38], and nonlinear loaded [39]. These various methods achieve wider bandwidth by engineering passive structures with various linear and nonlinear effects; however, they still do not achieve significant bandwidth increase. Moreover, most of those approaches are independent of power level in absorbing microwaves and in the struggle to suppress the surface waves due to the impinged fields.

B. High-Power Dependence

The proposed metasurface is designed to have a threshold power level to absorb the incident waves, that is, only the high-power signals are strongly absorbed, which are capable of being a trigger to make malfunction or damage by interfering with the sensitive electronic systems. In addition, surface currents induced from the impinged field on a metallic structure are allowed to propagate on a conductive surface and may interfere with the internal devices through a tiny aperture on the enclosure, which can be such a slot antenna to radiate inside. The traditional absorbers neither simply resolve these issues by covering them over the entire structure nor effectively mitigate the leakage currents due to its linearity [40]. Moreover, those passive absorbers can degrade the performance of the communication systems due to their power independent linearity in absorbing signals.

The HIS is well known to suppress the surface currents due to its unique boundary condition, $H_t = 0$ (tangential magnetic field is infinitesimal) instead of $E_t = 0$ at a conductive boundary, which does not support to propagate a current over the surface. Although the engineered structure has the advantage to suppress the surface waves over the traditional microwave absorbers, the HIS may cause another problem. It behaves like a resonator that can store energy from the incident waves. The energy, however, is not dissipated by the surface, so it can be either scattered to free space or reflected by nearby other parts, which may form standing waves. Most importantly, the HIS can vary a boundary condition nearby communication systems, which can affect their radiating performance and scattering properties, since it provides the artificial magnetic conducting boundary over the surface. The proposed surface can transform as the microwave absorber as assigning lossy components and have a power dependence by deploying the active RF components on it. Thus, the power dependence is not only suppressing the surface currents and dissipating incoming waves to protect against the high inputs, but also it cannot interrupt the scattering properties of the RF systems. Therefore, an important aspect, of the self-tuning metasurface is the absorptive behavior under the high powers, and it has decoupled to low-power boundary condition as an ordinary metallic surface, without any performance degradation of the communication systems.

III. Numerical Methods for Self-Tuning Mechanism

A. EM Unit Cell and Control Voltages

The active self-tuning metasurface can be modeled as a distributed array of LC circuits, where the capacitance is

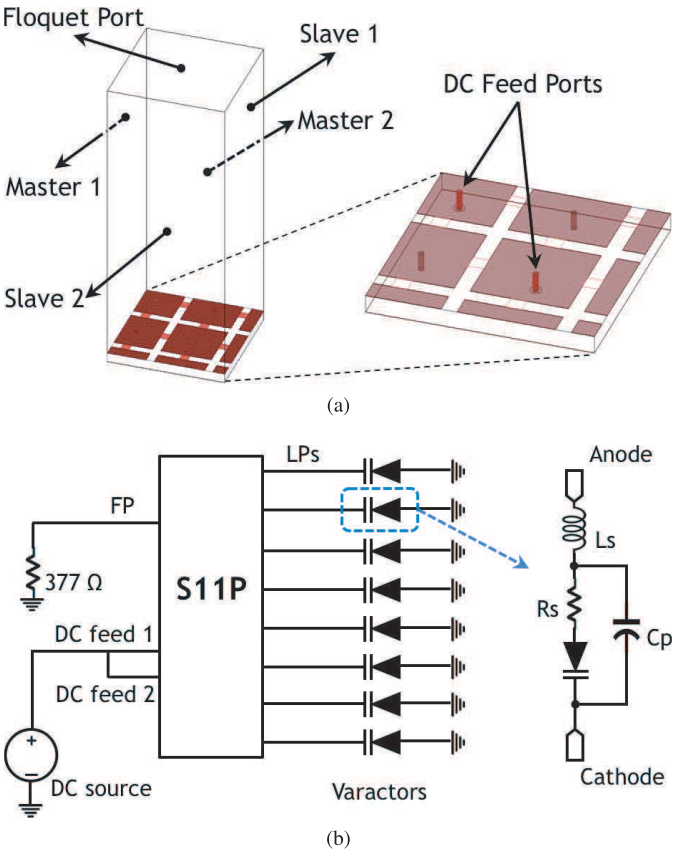

Fig. 1. EM and circuit cosimulation. (a) Offset EM unit-cell structure in Ansys HFSS Driven Modal with periodic conditions, Master and Slave boundaries, to the walls and a Floquet port on top. DC feed ports alternately neighbored to apply DC bias and lumped ports deployed between the top patches for varactor diodes in the zoomed inset. (b) Cosimulation circuit scheme linked to the extracted S-parameter touch stone (S11P) file with the varactor diodes. Inset: a SPICE model of the varactor.

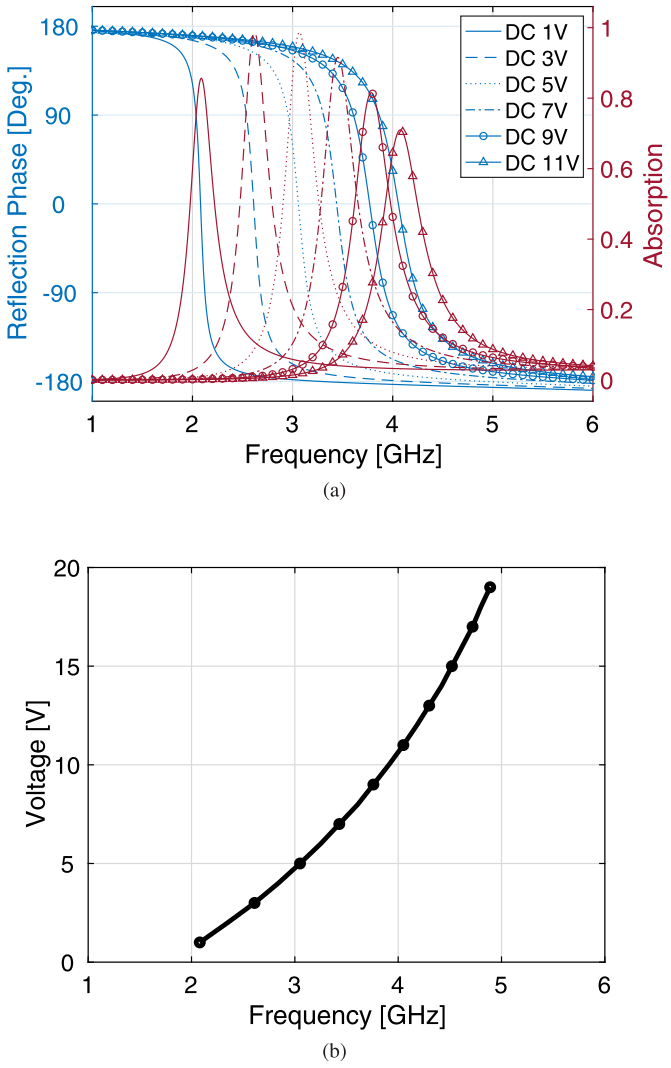

Fig. 2. Cosimulation data from the unit cell structure. (a) Reflection phase and absorption versus frequency while applying DC voltages in the cosimulation. Reflection phase and absorption magnitude are labeled in left and right y-axis, respectively. (b) Extracted control voltages versus frequency, which tune the resonance frequency of the metasurface.

determined by the gaps between neighboring metallic patches and the varactors, and the inductance is determined by the thickness of the substrate and periodicity of the patch. To extract proper control voltages to tune the varactor diodes, we perform an EM simulation for a unit cell and a cosimulation with a SPICE model of the varactor.

The periodic boundary conditions, master and slave boundaries to the facing walls, were applied to the unit cell model shown in Fig. 1(a) with a topped Floquet port and lumped ports at the gap. The unit cell was constructed by 2×2 subunit cell, which has 10 mm periodicity with 1.4 mm gap between cells and 1.575 mm of the dielectric substrate (Rogers RO5880), with an offset to avoid an intersection of the lumped ports by the periodic walls. Otherwise, the nonlinear components cannot apply to EM-circuit cosimulation due to an electrical discrepancy. In the bottom, note that a metallic via passing through a hole in the ground layer was centered on the metallic patch to supply bias to all of the varactor diodes deployed on the surface. Half of the patches were biased, and the other half were grounded by the neighboring vias, that is, the periodic unit cell is patterned like a checkerboard. Each unit cell was bridged by the varactor diodes to its four neighbors, and the diodes deployed in opposite directions in each alternate row were reversely biased. S-parameter data extracted from the full-wave EM simulation of the unit cell model in Fig. 1(a) are pulled into the circuit simulation with a SPICE model of the varactor diode for the cosimulation conducted by Ansys EDT, as shown in Fig. 1(b). The proposed metasurface uses a frequency demodulator circuit to allow control over its surface impedance and resonance frequency, through the use of varactor diodes attached between adjacent unit cells. To adjust the resonance frequency of the EM unit cell in the operation frequency from 2 to 5 GHz, the desired capacitance variation is from 2 to 0.2 pF, and SMV2019-079LF was selected as the varactor diode. Note that the SPICE model is shown in the inset and assigned to parasitic values, R_S 4.8 Ω of series resistance, L_s 0.7 nH of series inductance, and C_p 0.07 pF of parallel capacitance, respectively. The internal resistance of the diode plays a role of the loss factor to dissipate stored energy in each unit cell. The parasitic resistance in the varactors provides enough absorption as the loss term, but it may be not reliable depending on fabrication processes and selection of the varactor diode. In further research, one may need

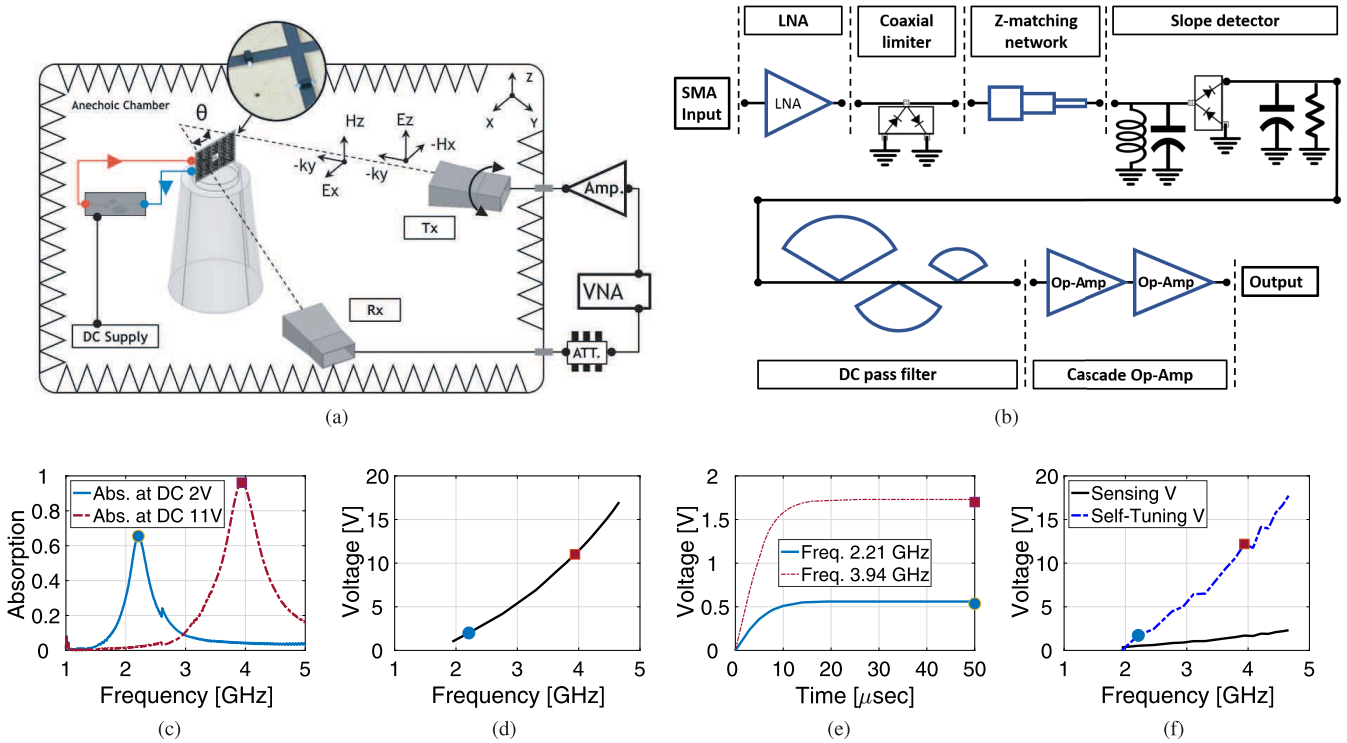

(a) (b) (c) (d) (e) (f)

Fig. 3. (a) Diagram of the measurement setup for the self-tuning surface. Inset of the metasurface with the varactors. (b) Flowchart of the sensing circuit. Cosimulation data for the self-tuning mechanism by following the flowchart. (c) Absorption of individual DC biasing, 2 and 11 V. (d) Required voltages in frequencies by assigning DC bias to apply the varactors. (e) Rectified signals at 2.21 and 3.94 GHz after passing through the slope detector. (f) Amplified control voltages in frequencies from the rectified signals to match the required voltages.

to consider modifying the structure to improve the stability of power dissipation. In the circuit scheme, DC sources are applied to have the desired control voltages versus frequency, and the Floquet port is terminated to free space characteristic impedance: 377 Ω. By addressing the unit cells in a single group, the reflection phase and absorption of the metasurface can be adapted in-phase as a function of applied voltages across the surface.

By biasing DC sources to the cosimulation scheme in Fig. 1(b), the total capacitance combined with an intrinsic capacitance from the gaps of the EM model and adding one from the varactor diodes can be varied to tune the resonance frequency of the surface. Reflection phase variation reveals that the resonance frequency of the surface is shifted by applying the DC voltages, and the absorption peak is associate with the resonance frequency, as shown in Fig. 2(a). In the plot, the applied DC bias varies from 1 to 11 V, and the absorption peaks are almost coincident with the reflection phase shift. From the phenomenon, we can extract a frequency point of the peak absorption associated with a specific bias voltage. For instance, 2.08 GHz peak frequency is from 1 V DC biasing in Fig. 2(a). The collected peak frequency points correlated with the DC bias voltages represent the desired control voltages to tune the metasurface, as shown in Fig. 2(b). The control voltages will be produced by a self-tuning circuit to give the self-tunability without any external controls.

B. Self-Tuning Metasurface and Closed-Loop Measurement

The measurement technique and self-tuning control circuit are shown in Fig. 3. The closed-loop measurement setup is shown in Fig. 3(a), including an anechoic chamber, a high-power amplifier, a vector network analyzer, and transmit (Tx) and receive (Rx) antennas. The Tx and Rx antennas were located 0.8 m from the self-tuning metasurface and rotated to 90° to provide the vertical and horizontal polarized plane waves. The angle between the two antennas was varied from normal to 60°. For normal incidence, both antennas were located very close together, and a thin (about 3 cm) absorbing foam was placed between the antennas. The foam provides isolation between the two antennas of 50 dB. A circularly polarized patch antenna is located near the center of the surface, which samples the incoming waves for either linear polarization. Unlike a conventional patch antenna, the antenna was designed as a sensing cell with a very low Q-factor to respond over a broad frequency band, that is, the received power level was stabilized over the operating frequency band to minimize power dependence in a sensing circuit response. A buffer region was also required around the antenna, because the received power near a resonance frequency at the patch was otherwise sensitive to the tuning state of the surface. Fig. 3(b) exhibits a flowchart of the sensing circuit. The output of the patch is fed to a cascaded pair of low noise amplifiers and a coaxial limiter (Krytar KSL), which sets the power level going into the slope detector circuit. This is required to remove any dependence on the power level of the input signal, ensuring that the feedback circuit is primarily responsive to frequency. The slope detector consists of an LC circuit tuned to provide linear frequency response, a pair of series diodes to rectify the RF signals to DC, and a shunt capacitor and potentiometer as a variable load. Impedance matching

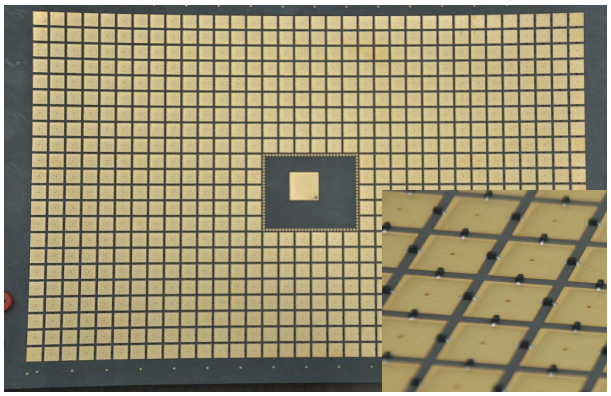

(a)

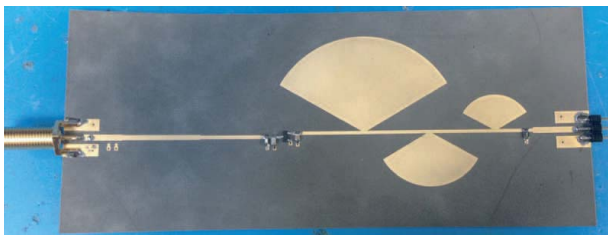

(b)

Fig. 4. Photographs of the self-tuning metasurfaces. (a) Photograph of the top surface of the prototype self-tuning metasurface. The sensing antenna is located at the center of the board. Inset: varactor diodes populated between the top patches. (b) Photograph of the self-tuning circuit board.

networks and a low-pass filter consisting of radial stubs are also used to optimize transmission and prevent leakage RF or harmonic signals into the final signal conditioning part of the circuit. A pair of op-amps provide a DC offset and gain so that the response of the control circuit matches that of the tunable surface to complete the feedback loop. The feedback circuit is designed to match the voltage–frequency response of the absorbing metasurface, as shown in Fig. 3(c)–(f). The capacitance between each pair of unit cells in the metasurface consists of a parallel combination of the junction capacitance of the varactor diodes, which is tunable, and the parasitic capacitance between the metal patches, which is constant. The resonance frequency in the absorption of the surface is given by $\omega_r = 1/\sqrt{LC_t}$, where C_t is the total capacitance, including the tunable and fixed components shown in Fig. 3(c). The required bias voltage on the varactors is determined from the diode C/V curves and then verified by electromagnetic/circuit cosimulation shown in Fig. 3(d). The rectified voltages at 2.21 and 3.94 GHz with 30 dBm are estimated by the cosimulation after passing through the slope detector shown in Fig. 3(e). To achieve optimized bias voltage over the tuning range of the metasurface, the final two op-amps in the feedback circuit are designed to provide a voltage gain of 9 and an offset of -3.1 V in Fig. 3(f). In addition, the closed-loop measurement for the metasurface was carried out to sweep continuous waves (CWs) due to a response time of the circuitry. The two main factors to drive the response speed of this metasurface are the time constant from the rectifying stage and the slew rate of the cascaded op-amps of the self-tuning circuit stage. In the rectifying stage, the time constant is 3 μs, and the slew rate of the op-amp, AD8597ARZ-ND, is 14 V/μs from a manufacturer datasheet. Thus, the response time of this metasurface is over 17 μs, and in the measurement CW with 1 second signal sources were assigned to have enough response time. The short pulse responses will be discussed in further research.

C. Fabricated Prototype Self-Tuning Metasurface

The fabricated metasurface shown in Fig. 4(a) has 718 periodic patches connected by 1369 varactor diodes in an area of 25 $\times$ 40 cm^2. It has three copper cladding layers and two dielectric layers. The upper dielectric material that forms the metasurface is Rogers RO5880 with a thickness of 1.575 mm, the second layer is ground plane with holes to pass through the biasing vias and a signal via of a sensing antenna, and the third layer that contains the bias lines is standard FR4 materials. The lower circuit layer also contains buffer amplifiers, BUF634, to ensure reliable control voltages are provided to each varactor and resistors to protect the varactors. The antenna located in the center of the surface samples the incoming waves, which are fed to a self-tuning circuit shown in Fig. 4(b), which converts the incoming frequency to a control voltage that is applied to the varactor diodes. The fabricated self-tuning circuit board has two copper layers with a thickness of 0.508 mm dielectric substrate, AL260L. The board has constructed with the quarter-wave impedance matching network to a rectifying diode, lumped components for parallel LC resonator, the rectifying diode, HSMS-2822, and three radial open stubs to reject higher harmonics to generate DC outputs. By matching the frequency–voltage response of the feedback circuit to the voltage–frequency response of the tunable metasurface, the combined structure automatically self-tunes its resonance frequency to match that of the incoming waves.

IV. Measurement Results

The metasurface was measured under various conditions to verify its absorbing characteristics, as shown in Figs. 5 and 6. The proposed metasurface is the grounded structure, and the Tx and Rx antennas are located on the same side, as shown in Fig. 3(a), so the transmitted waves are reflected by the metallic layer of the board. Therefore, the absorption is dominantly determined by the transmission coefficient, that is, the lowest transmission peak can be considered the highest absorption point. The transmission coefficient results are relative magnitude in dB scale, using a calibration procedure. The calibration was carried out under the same test condition using a metallic plane of the same size as the metasurface. Before conducting the closed-loop measurement, an open-loop measurement had been carried out by biasing DC voltages to the metasurface to tune the varactors. In the open-loop measurement, the high-power incident waves to the threshold power level are not necessary due to biasing by an external DC supply; thus, the high-power amplifier shown in Fig. 3(a) was not used. The measured transmission coefficient data is shown in Fig. 5(a) and (b), and the individual thin curves represent the

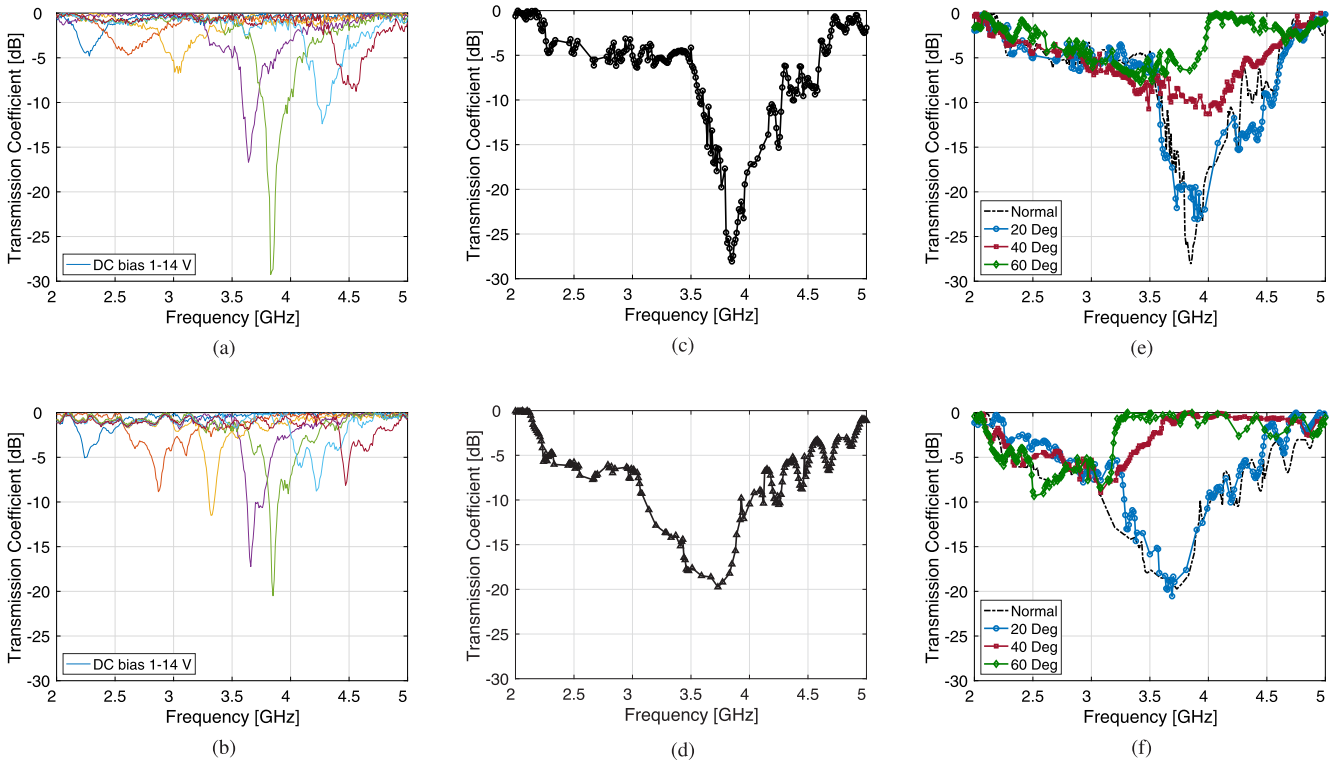

Fig. 5. Transmission coefficient by DC biasing from 1 to 14 V for (a) vertical- and (b) horizontal-polarized plane waves. The thin solid lines represent the instantaneous absorption. Transmission coefficient of the self-tuning metasurface by the self-tuning biasing for (c) vertical- and (d) horizontal-polarized plane waves. The curves represent the self-tuning absorption characteristics of the self-tuning metasurface under different measurement conditions. Varying incident angles: normal, 20°, 40°, and 60° in (e) TE and (f) TM incident waves.

absorption band of the surface for various values of bias voltages from 1 to 14 V on the varactors which are set manually. Note that the plots are selected for some of the bias voltage cases. As increasing DC bias from 1 to 14 V, the absorption peak is shifted to the higher frequency as varying the junction capacitance of the varactors. This open-loop measurement can provide a guideline for the absorption of the self-tuning under the closed-loop test. In Fig. 5(c) and (d), the plots exhibit the absorption of the self-tuning metasurface for normally incident vertical- and horizontal-polarized waves, respectively. Because the sensing antenna is circularly polarized, it responds to incoming waves of both linear polarizations. Fig. 5(c)–(f) for the closed-loop measurement were plotted at 41 dBm of the input power by varying from 10 to 47 dBm, and the frequency of the incident CW was swept from 2 to 5 GHz. The power density calculated from the test environment is 0.1–215.4 mW/cm^2 corresponding to the swept incident powers. The bold curves in Fig. 5(c) and (d) represent the response of the surface when the self-tuning circuit is turned on. The both curves differently polarized in Fig. 5(c) and (d) show a good agreement with Fig. 5(a) and (b), respectively. The absorption frequency range of the self-tuning surface is about 70% compared wih instantaneous fractional frequency range around 5% for each individual tuning state, as listed in Table I. The frequency range defined by the -3 dB transmission coefficient of the metasurface spans from 2.26 to 4.69 GHz at the center frequency of 3.8 GHz for the vertical-polarized case and from 2.21 to 4.89 GHz at the center frequency of 3.73 GHz for the horizontal-polarized case from Table I corresponding to the fractional frequency range of 63.9% and 71.8% calculated as $\triangle f/f_c$, respectively. Here, $\triangle f$ is defined by subtracting f_L, the lower edge, from f_H, the higher one, at the -3 dB boundary frequencies. The magnitude of absorption varies slightly over its operating band due to the nonlinearity of the varactor diodes. Changing the bias voltage varies both the junction capacitance and the series resistance, which affects the absorption of the surface.

In general, microwave absorbers are designed to perform optimally near normal incidence, but they must still be capable of addressing incident waves over a range of angles, ideally down to oblique incidence. The self-tuning metasurface is able to respond to incoming wave at oblique angles to the surface. Fig. 5(e) and (f) shows the absorption for various angles of incidence up to 60° in TE- and TM-polarized incident waves, respectively. The surface maintains its self-tuning properties; however, the frequency range is diminished at higher angles due to the angle dependence of the intrinsic surface impedance and resonance frequency. The measurements were performed in the near-field, so the incident waveform at the metasurface may not be an exact plane wave. In other words, the wavefront at the sample may have some angle dependence. Although the metasurface has shown its absorbing performance over a certain range of incident angles in Fig. 5(e) and (f), some

TABLE I
3 dB FRACTIONAL FREQUENCY RANGE PERCENTAGE OF THE SELF-TUNING METASURFACE

Status	f_c [GHz]	f_L [GHz]	f_H [GHz]	BW [%]
Vertical Pol.				
DC 1V	2.28	2.19	2.35	7.0
DC 8V	3.83	3.67	4.18	13.3
DC 14V	4.56	4.36	4.72	7.8
Self-Tuning	3.8	2.26	4.69	63.9
Horizontal Pol.				
DC 1V	2.24	2.21	2.36	6.6
DC 8V	3.85	3.66	4.1	11.4
DC 14V	4.47	4.42	4.7	6.2
Self-Tuning	3.73	2.21	4.89	71.8
Case	f_c [GHz]	**Thickness**		BW [%]
Ref. [17]	10	1 mm		18
Ref. [24]	3.5 - 4.5	1.6 mm		8
Ref. [41]	6.5	2 mm		15.3
Ref. [42]	2.3	3 mm		17.3

amount of power may be scattered rather than being dissipated by the surface.

The surface impedance is given by $Z_s = j\omega L/(1 - \omega^2 LC)$, where the HIS is modeled as a parallel resonant LC circuit. The result is that the surface is capacitive above resonance, where it supports TE waves, and it is inductive below resonance, where it supports TM waves. The self-tuning mechanism of the metasurface is designed based on TE mode resonance to maximize the suppression of the surface currents. In the TE mode case, with increasing the incident angle up to 40° from normal, the absorption intensity remains similar to the normal incident case, while the self-tuned resonance frequency is barely shifted. Further increasing the incident angle over 40°, the resonance frequency of the self-tuning surface will vary and cause a shift in the resonance frequency, resulting in the divergence between the control voltages of the self-tuning circuit and the required voltages to the varactors. This decreases the intensity and frequency range of the absorption in Fig. 5(e). In the TM mode case, the absorption and frequency range of the metasurface is decreased even faster than the TE mode case while increasing the incident angles, as shown in Fig. 5(f). This is because the resonance frequency is shifted to lower frequencies faster for TM polarization, accelerating the divergence between the applied voltage and the optimum voltage for the varactors, resulting in a faster decrease in absorption performance than the TE mode incident. Although some discrepancy between TM performance and TE performance is typical of metasurfaces, the sensitivity of the self-tuning mechanism may limit the use of these structures in practical applications.

In addition, the surface is able to respond to a wide range of input powers. Fig. 6 shows the absorption of the surface by incident power density up to 100 mW/cm^2. The absorption was calculated as A(ω) = 1 - T(ω). (Here, A(ω): absorption, T(ω): transmission between Rx and Tx, and ω is an angular frequency.) At low powers, the absorption is diminished due to the threshold response of the rectifying diodes in the feedback circuit. At higher power levels, the absorption varies due to

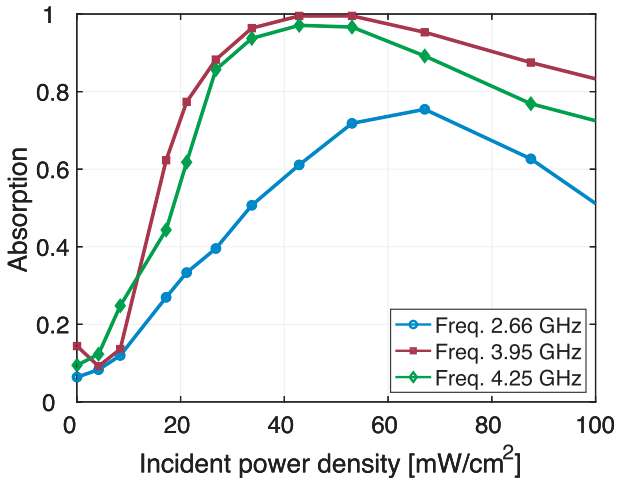

Fig. 6. Absorption magnitude variation versus incident power density with different frequencies at 2.66, 3.95, and 4.25 GHz.

the limitations of the limiter circuit. Nonetheless, over 90% of the absorption magnitude maintains wider incident power density levels between 25 and 60 mW/cm^2 for the higher frequency points: 3.95 and 4.25 GHz. The slight decrease of the absorbing magnitude over 70 mW/cm^2 is because of the power limit of the coaxial limiter. At the lower frequency at 2.66 GHz, the absorption magnitude is lower than at the higher frequencies due to the nonlinearity of the varactors although it still maintains the power dependence.

V. CONCLUSION

In this article, we have demonstrated a novel self-tuning metamaterial surface that provides a significantly greater frequency range compared with a passive absorbing surface of the same thickness. The surface is based on a resonant HIS that is tuned using varactor diodes and a simple feedback circuit that senses the frequency of the incoming waves and tunes the bias voltage on the varactors. The feedback circuit is based on a limiter and frequency demodulator, which provides a voltage that is proportional to the incoming frequency, with appropriate gain and offset voltage to match the response of the varactor-tuned surface. We have shown that the surface achieves about 70% absorbing fractional frequency range compared with 5% for each individual tuning state. In addition, the surface responds to both polarizations, as well as various incident angles and power levels. This self-tuning absorber circumvents the fundamental relationship between bandwidth and thickness for passive absorbers, which can potentially address a wide range of applications where a thin coating with broadband absorption to suppress the high-power surface currents is required. Moreover, the proposed metasurface is applicable to an active frequency detector based on its frequency modulation and a ground plane to support a massive MIMO antenna system as selectively decoupling between different operation bands.

REFERENCES

[1] R. E. Collin, *Foundations for Microwave Engineering*. Hoboken, NJ, USA: Wiley, 2007.
[2] K. N. Rozanov, "Ultimate thickness to bandwidth ratio of radar absorbers," *IEEE Trans. Antennas Propag.*, vol. 48, no. 8, pp. 1230–1234, Aug. 2000.

[3] B. A. Munk, *Frequency Selective Surfaces: Theory and Design*. Hoboken, NJ, USA: Wiley, 2000.
[4] W. W. Salisbury, "Absorbent body for electromagnetic waves," U.S. Patent 2 599 944, Jun. 10, 1952.
[5] R. L. Fante and M. T. McCormack, "Reflection properties of the salisbury screen," *IEEE Trans. Antennas Propag.*, vol. AP-36, no. 10, pp. 1443–1454, Oct. 1988.
[6] R. A. Gilbert, "Thin, broadband salisbury screen absorber," U.S. Patent 6 538 596, Mar. 25, 2003.
[7] B. A. Munk, P. Munk, and J. Pryor, "On designing jaumann and circuit analog absorbers (CA absorbers) for oblique angle of incidence," *IEEE Trans. Antennas Propag.*, vol. 55, no. 1, pp. 186–193, Jan. 2007.
[8] N. I. Zheludev and Y. S. Kivshar, "From metamaterials to metadevices," *Nature Mater.*, vol. 11, no. 11, p. 917, 2012.
[9] A. Li, Z. Luo, H. Wakatsuchi, S. Kim, and D. F. Sievenpiper, "Nonlinear, active, and tunable metasurfaces for advanced electromagnetics applications," *IEEE Access*, vol. 5, pp. 27439–27452, 2017.
[10] S. B. Glybovski, S. A. Tretyakov, P. A. Belov, Y. S. Kivshar, and C. R. Simovski, "Metasurfaces: From microwaves to visible," *Phys. Rep.*, vol. 634, pp. 1–72, May 2016.
[11] H.-T. Chen, A. J. Taylor, and N. Yu, "A review of metasurfaces: Physics and applications," *Rep. Prog. Phys.*, vol. 79, no. 7, Jun. 2016, Art. no. 076401.
[12] A. Li, S. Singh, and D. Sievenpiper, "Metasurfaces and their applications," *Nanophotonics*, vol. 7, no. 6, pp. 989–1011, Jun. 2018.
[13] F. Costa, A. Monorchio, and G. Manara, "An equivalent-circuit modeling of high impedance surfaces employing arbitrarily shaped FSS," in *Proc. Int. Conf. Electromagn. Adv. Appl.*, Sep. 2009, pp. 852–855.
[14] S. Clavijo, R. E. Diaz, and W. E. McKinzie, "Design methodology for sievenpiper high-impedance surfaces: An artificial magnetic conductor for positive gain electrically small antennas," *IEEE Trans. Antennas Propag.*, vol. 51, no. 10, pp. 2678–2690, Oct. 2003.
[15] Y. Pang, H. Cheng, Y. Zhou, and J. Wang, "Upper bound for the bandwidth of ultrathin absorbers comprising high impedance surfaces," *IEEE Antennas Wireless Propag. Lett.*, vol. 11, pp. 224–227, 2012.
[16] H.-B. Zhang, P.-H. Zhou, H.-P. Lu, Y.-Q. Xu, D.-F. Liang, and L.-J. Deng, "Resistance selection of high impedance surface absorbers for perfect and broadband absorption," *IEEE Trans. Antennas Propag.*, vol. 61, no. 2, pp. 976–979, Feb. 2013.
[17] F. Costa, A. Monorchio, and G. Manara, "Analysis and design of ultra thin electromagnetic absorbers comprising resistively loaded high impedance surfaces," *IEEE Trans. Antennas Propag.*, vol. 58, no. 5, pp. 1551–1558, May 2010.
[18] P. Mei, S. Zhang, X. Q. Lin, and G. F. Pedersen, "A triple-band absorber with wide absorption bandwidths using an impedance matching theory," *IEEE Antennas Wireless Propag. Lett.*, vol. 18, no. 3, pp. 521–525, Mar. 2019.
[19] M. Yoo and S. Lim, "Polarization-independent and ultrawideband metamaterial absorber using a hexagonal artificial impedance surface and a resistor-capacitor layer," *IEEE Trans. Antennas Propag.*, vol. 62, no. 5, pp. 2652–2658, May 2014.
[20] F. Costa, S. Genovesi, A. Monorchio, and G. Manara, "A circuit-based model for the interpretation of perfect metamaterial absorbers," *IEEE Trans. Antennas Propag.*, vol. 61, no. 3, pp. 1201–1209, Mar. 2013.
[21] D. Zhirihin, C. Simovski, P. Belov, and S. Glybovski, "Mushroom high-impedance metasurfaces for perfect absorption at two angles of incidence," *IEEE Antennas Wireless Propag. Lett.*, vol. 16, pp. 2626–2629, 2017.
[22] F. Costa and A. Monorchio, "Multiband electromagnetic wave absorber based on reactive impedance ground planes," *IET Microw., Antennas Propag.*, vol. 4, no. 11, pp. 1720–1727, Nov. 2010.
[23] A. Li, S. Kim, Y. Luo, Y. Li, J. Long, and D. F. Sievenpiper, "High-power transistor-based tunable and switchable metasurface absorber," *IEEE Trans. Microw. Theory Techn.*, vol. 65, no. 8, pp. 2810–2818, Aug. 2017.
[24] D. F. Sievenpiper, J. H. Schaffner, H. J. Song, R. Y. Loo, and G. Tangonan, "Two-dimensional beam steering using an electrically tunable impedance surface," *IEEE Trans. Antennas Propag.*, vol. 51, no. 10, pp. 2713–2722, Oct. 2003.
[25] C. Mias and J. H. Yap, "A varactor-tunable high impedance surface with a resistive-lumped-element biasing grid," *IEEE Trans. Antennas Propag.*, vol. 55, no. 7, pp. 1955–1962, Jul. 2007.
[26] F. Costa, A. Monorchio, S. Talarico, and F. M. Valeri, "An active high-impedance surface for low-profile tunable and steerable antennas," *IEEE Antennas Wireless Propag. Lett.*, vol. 7, pp. 676–680, 2008.
[27] F. Costa, A. Monorchio, and G. P. Vastante, "Tunable high-impedance surface with a reduced number of varactors," *IEEE Antennas Wireless Propag. Lett.*, vol. 10, pp. 11–13, 2011.
[28] D. Cure, T. M. Weller, and F. A. Miranda, "Study of a low-profile 2.4-GHz planar dipole antenna using a high-impedance surface with 1-D varactor tuning," *IEEE Trans. Antennas Propag.*, vol. 61, no. 2, pp. 506–515, Feb. 2013.
[29] Z. Luo, X. Chen, J. Long, R. Quarfoth, and D. Sievenpiper, "Nonlinear power-dependent impedance surface," *IEEE Trans. Antennas Propag.*, vol. 63, no. 4, pp. 1736–1745, Apr. 2015.
[30] C. L. Holloway, R. R. DeLyser, R. F. German, P. McKenna, and M. Kanda, "Comparison of electromagnetic absorber used in anechoic and semi-anechoic chambers for emissions and immunity testing of digital devices," *IEEE Trans. Electromagn. Compat.*, vol. 39, no. 1, pp. 33–47, Feb. 1997.
[31] B.-K. Chung and H.-T. Chuah, "Modeling of RF absorber for application in the design of anechoic chamber," *Prog. Electromagn. Res.*, vol. 43, pp. 273–285, Jan. 2003.
[32] Y. Naito and K. Suetake, "Application of ferrite to electromagnetic wave absorber and its characteristics," *IEEE Trans. Microw. Theory Techn.*, vol. MTT-19, no. 1, pp. 65–72, Jan. 1971.
[33] S. Kim, H. Wakatsuchi, J. J. Rushton, and D. F. Sievenpiper, "Switchable nonlinear metasurfaces for absorbing high power surface waves," *Appl. Phys. Lett.*, vol. 108, no. 4, Jan. 2016, Art. no. 041903.
[34] H. Wakatsuchi, S. Kim, J. J. Rushton, and D. F. Sievenpiper, "Waveform-dependent absorbing metasurfaces," *Phys. Rev. Lett.*, vol. 111, no. 24, Dec. 2013, Art. no. 245501.
[35] D. Sievenpiper, L. Zhang, R. F. J. Broas, N. G. Alexopolous, and E. Yablonovitch, "High-impedance electromagnetic surfaces with a forbidden frequency band," *IEEE Trans. Microw. Theory Techn.*, vol. 47, no. 11, pp. 2059–2074, Nov. 1999.
[36] C. A. Balanis, *Modern Antenna Handbook*. Hoboken, NJ, USA: Wiley, 2008.
[37] D. F. Sievenpiper, "High impedance electromagnetic surfaces," Ph.D. dissertation, Dept. Elect. Eng., Univ. California Los Angeles, Los Angeles, CA, USA, 1999.
[38] H. Xiong, J.-S. Hong, C.-M. Luo, and L.-L. Zhong, "An ultrathin and broadband metamaterial absorber using multi-layer structures," *J. Appl. Phys.*, vol. 114, no. 6, Aug. 2013, Art. no. 064109.
[39] D. A. Powell, I. V. Shadrivov, Y. S. Kivshar, and M. V. Gorkunov, "Self-tuning mechanisms of nonlinear split-ring resonators," *Appl. Phys. Lett.*, vol. 91, no. 14, Oct. 2007, Art. no. 144107.
[40] D. F. Sievenpiper, "Nonlinear grounded metasurfaces for suppression of high-power pulsed RF currents," *IEEE Antennas Wireless Propag. Lett.*, vol. 10, pp. 1516–1519, 2011.
[41] A. Kazemzadeh and A. Karlsson, "On the absorption mechanism of ultra thin absorbers," *IEEE Trans. Antennas Propag.*, vol. 58, no. 10, pp. 3310–3315, Oct. 2010.
[42] S. Tretyakov and S. Maslovski, "Thin composite radar absorber operational for all incidence angles," in *Proc. 33rd Eur. Microw. Conf.*, vol. 3, Oct. 2003, pp. 1107–1110.

Sanghoon Kim (Member, IEEE) received the B.S. and M.S. degrees in physics from Konkuk University, Seoul, South Korea, in 2005 and 2008, respectively, and the Ph.D. degree from the University of California at San Diego (UC San Diego), La Jolla, CA, USA, in 2017. At UC San Diego for pursuing the Ph.D. degree, he had focused on nonlinear active metasurfaces for electromagnetic absorber and reconfigurable impedance surfaces.

In 2017, he joined the antenna industry fields. His research interests are applied electromagnetics, advanced metamaterials, phased-array and reflector antennas, and satellite communications.

Aobo Li (Member, IEEE) received the B.S. degree from Shanghai Jiao Tong University, Shanghai, China, in 2010, the dual M.S. degree in electrical engineering and telecommunications from Shanghai Jiao Tong University (SJTU), Shanghai, China, and the Georgia Institute of Technology, Atlanta, GA, USA, respectively, in 2013, and the Ph.D. degree in electrical engineering from the University of California at San Diego, La Jolla, CA, USA, in 2018.

From 2013 to 2014, he worked as an Application Engineer with National Instruments, Austin, TX, USA. His research focuses on advanced electromagnetics applications, including active metasurface microwave absorbers, metasurface microwave sources, wireless power transmission, and phased arrays systems.

Jiyeon Lee (Member, IEEE) received the B.S. degree from Hongik University, Seoul, South Korea, in 2007, and the M.S. and Ph.D. degrees from the University of California at San Diego, La Jolla, CA, USA, in 2013 and 2018, respectively.

From 2008 to 2011, she was a Software Engineer of the MIS system at SK C&C, Seoul. Her research interests include artificial impedance surfaces, metamaterials, antennas, and communication circuits.

Daniel F. Sievenpiper (Fellow, IEEE) received the B.S. and Ph.D. degrees in electrical engineering from the University of California at Los Angeles, Los Angeles, CA, USA, in 1994 and 1999, respectively.

He joined HRL Laboratories, Malibu, CA, USA, in 1999. During the following 11 years, he and his team developed new electromagnetic structures with an emphasis on small, conformal, tunable, and steerable antennas. He held a variety of technical and management positions at HRL Laboratories, Malibu, CA, USA, including the Director of the Applied Electromagnetics Laboratory. In 2010, he joined UC San Diego as a Professor with the Electrical and Computer Engineering Department, where his research is focused on artificial media, and the integration of active electronics with electromagnetic structures and antennas to enable new capabilities and applications. He holds more than 70 issued patents and more than 150 publications. His recent work involves anisotropic and active metasurfaces, photonic and phononic topological insulators, small and wearable antennas, and biological applications of electromagnetics.

Dr. Sievenpiper received the URSI Issac Koga Gold Medal and also the IEEE Antennas and Propagation Society Piergiorgio Uslenghi Letters Prize Paper Award in 2008. In 2019, he was awarded the John D. Kraus Antenna Award. He also served as the Chair for the IEEE Antennas and Propagation Society Administrative Committee on New Technology Directions from 2013 to 2014 and the General Chair for the IEEE Antennas and Propagation Symposium and URSI Radio Science Meeting which was held in San Diego in 2017. Beginning in 2019, he has served as the Vice-Chair for the UCSD Electrical and Computer Engineering Department. From 2010 to 2017, he served as an Associate Editor for the IEEE ANTENNAS AND WIRELESS PROPAGATION LETTERS.